Journal of Alloys and Compounds 480 (2009) 706–710

Contents lists available at ScienceDirect

Journal of Alloys and Compounds

journal homepage: www.elsevier.com/locate/jallcom

Yb^{3+}–Er^{3+} co-doped sol–gel transparent nano-glass-ceramics containing $NaYF_4$ nanocrystals for tuneable up-conversion phosphors

A.C. Yanes [a,*], A. Santana-Alonso [a], J. Méndez-Ramos [b], J. del-Castillo [a], V.D. Rodríguez [b]

[a] Dpto. Física Básica, Universidad de La Laguna, 38206 La Laguna, Tenerife, Spain
[b] Dpto. Física Fundamental y Experimental, Electrónica y Sistemas, Universidad de La Laguna, 38206 La Laguna, Tenerife, Spain

ARTICLE INFO

Article history:
Received 18 December 2008
Received in revised form 4 February 2009
Accepted 6 February 2009
Available online 20 February 2009

Keywords:
Nano-glass-ceramics
Sol–gel
Up-conversion
Color tuneability

ABSTRACT

Transparent nano-glass-ceramics containing Yb^{3+}–Er^{3+} co-doped $NaYF_4$ nanocrystals have been successfully developed for the first time by thermal treatment of precursor bulk glasses obtained by sol–gel technique. Precipitation of $NaYF_4$ nanocrystals has been confirmed by X-ray diffraction measurements and their sizes have been determined by Scherrer's equation. Luminescence measurements confirm the partition of rare-earth ions in $NaYF_4$ nanocrystals. Visible up-conversion luminescence has been obtained under infrared excitation at 980 nm. Up-conversion mechanisms have been discussed and the ratio between red and green up-conversion emission bands can be varied as a function of temperature of heat treatment and pump power resulting in colour tuneable up-conversion phosphors with applications in optical integrated devices. Colour tuneability has been also analyzed and quantified in terms of CIE standard chromaticity diagram.

1. Introduction

Rare-earth (RE) doped transparent nanostructured oxyfluoride glass-ceramics can be prepared by either heat treatment of precursor glasses or by direct laser writing within the bulk of these glasses [1–5], inducing a controlled crystallization of low phonon energy fluoride nanocrystalline phase embedded among the oxide glassy matrix. Due to nano-scale size of fluoride crystals the material remains transparent since light scattering is avoided. RE ions are selectively incorporated during thermal treatment into these fluoride nanocrystals [1,4,6], and therefore the luminescence properties can be enhanced [7,8]. Thus, nanomaterials doped with RE ions have attracted great interest in recent years due to their applications in fields such as tuneable infrared phosphors for three-dimensional optical recording [1,8], white light generation for ambient lighting and displays, solid-state lasers and solar cells [9–13] and biological labels [14–16].

$NaYF_4$ crystal is known to be one of the most efficient RE ions host for near infrared to visible up-conversion. In this sense, RE doped up-converting phosphors based on micrometer-sized $NaYF_4$ powders were studied by Suyver et al. [10,11] and found to be useful for enhanced response in the near-infrared for silicon solar cells [13] due to high efficiency up-conversion processes. On the other hand, $NaYF_4$ nanoparticles have been successfully used as nanophosphors for bioimaging [14], near infrared photodetectors [17], sensitive detection of DNA [15] and biological fluorescent probe labelling among current nanobiotechnology research developments [16,18,19].

In particular, infrared to visible up-conversion processes can be obtained by means of energy transfer when doping with Yb^{3+}/Er^{3+} couple [20–24]. Moreover, the ratio between red and green up-conversion emission bands can be varied resulting in colour tuneable up-conversion phosphors with applications in optical integrated devices [8,10,11,25–27].

Recently, transparent glass-ceramics comprising Er^{3+} and Nd^{3+} doped $NaYF_4$ nanocrystals have been successfully synthesized by conventional melting technique at 1450 °C, studying up-conversion processes [28], crystallization kinetics, microstructure and spectroscopic properties [29,30].

Highly transparent nanostructured RE doped glass-ceramics have been obtained by the authors in previous works under thermal treatment of precursor glasses prepared by room temperature sol–gel method, carrying out a structural analysis and a spectroscopic study by means of X-ray diffraction measurements, transmission electron microscopy along with emission and excitation spectra [31–33]. This method permits the incorporation of RE ions into the precipitated nanocrystals within the sample (SnO_2 and LaF_3 in the case of [31–33], respectively) under controlled concentration and size. Site selective and time resolved measurements allowed the authors to discern between ions in glassy and nanocrystalline environments, analyzing energy transfer mechanisms and up-conversion processes.

* Corresponding author. Tel.: +34 922 318 304; fax: +34 922 318 228.
E-mail address: ayanesh@ull.es (A.C. Yanes).

0925-8388/$ – see front matter © 2009 Elsevier B.V. All rights reserved.
doi:10.1016/j.jallcom.2009.02.019

Finally, in this work, we present for the first time sol–gel derived transparent nano-glass-ceramics comprising Er^{3+} and Yb^{3+} co-doped $NaYF_4$ nanocrystals. A structural and luminescence study has been carried out focusing the attention in up-conversion processes and tuneability of emitting colour. In particular, we investigate how the ratio of the red to green up-conversion emissions varies with the pump power and with the heat treatment of the precursor glass. The observed colour tuneability is important from the viewpoint of applications for this material such as solid-state lasers and 3D optical recording for enhanced memory storage devices. Current research is being carried out by the authors in Eu^{3+} single doped samples to investigate the incorporation of these RE ions to the precipitated $NaYF_4$ nanocrystals by site selective luminescence.

2. Experimental

Silica glasses with compositions of $95SiO_2$–$5NaYF_4$ co-doped with 0.1 mol% of Er^{3+} and 0.3 mol% of Yb^{3+} were synthesized by a sol–gel procedure in a similar way to that of Fujihara et al. [34]. First, tetraethoxysilane (TEOS) was hydrolyzed for 1 h at room temperature with a mixed solution of ethanol and H_2O, using acetic acid as a catalyst. The molar ratio of TEOS:ethanol:H_2O:CH_3COOH was 1:4:10:0.5. The required quantity of $Y(CH_3COO)_3{\cdot}xH_2O$, $NaCH_3COO$, $Er(CH_3COO)_3{\cdot}xH_2O$ and $Yb(CH_3COO)_3{\cdot}xH_2O$ were dissolved in CF_3COOH and H_2O solution, which was slowly mixed with the initial solution. The molar ratio of metal ions to CF_3COOH was 1:4. Transparent sols were obtained after stirring vigorously for 1 h at room temperature. A wet-gel was obtained by leaving the solution in a sealed container at 35 °C for 1–2 weeks. After this step, evaporation for several weeks at 35 °C was required to obtain dried samples, known as xerogels. Finally, these xerogels were heat-treated in air at different temperatures ranging from 550 to 650 °C in order to achieve controlled precipitation of nanocrystallites, giving rise to a transparent glass-ceramic.

X-ray diffraction patterns (XRD) were carried out by using a Cu anode (Cu $K\alpha_{1,2}$) in the 10–90 2-Theta range. Measurements were corrected by using LaB_6.

Luminescence measurements were obtained by exciting the samples with light from a 75 W Xe arc lamp, passed through a 0.25 m monochromator and detecting with a 0.25 m monochromator with a photomultiplier. The up-conversion spectra were obtained under 980 nm laser excitation with a power up to 200 mW focused with a microscope objective with 3 mm focal length. All spectra were collected at room temperature and corrected by the instrumental response.

3. Results and discussion

3.1. Structural characterization

A structural characterization in terms of X-ray diffraction (XRD) measurements has been carried out in these $95SiO_2$–$5NaYF_4$ co-doped with 0.3 Yb^{3+} and 0.1 Er^{3+} (mol%) transparent sol–gel derived nano-glass-ceramics. Fig. 1 presents XRD patterns as a function of heat treatment temperature ranging from 550 to 650 °C, corresponding to precipitation of cubic $NaYF_4$ nanocrystals (JCPDS No. 06-0342) with no second crystalline phase. It can be noticed how the diffraction peaks become sharper and more intense, indicative of a higher degree of crystallinity with increasing temperature of the thermal treatment. In that respect, from the width of the XRD peaks, the size of the nanocrystals in the obtained nano-glass-ceramic can be calculated by using Scherrer's equation

$$D = \frac{K\lambda}{\beta \cos\theta} \quad (1)$$

where D is the crystal size, λ the X-ray wavelength, θ the diffraction angle, β the full-width at half-maximum (FWHM) of the diffraction peak and K a constant determined by the instrument. Calculated nanocrystals average radii (in nm) for different samples are presented in Table 1 showing up the increase of the radius of precipitated $NaYF_4$ nanocrystals with the treatment temperature, ranging from 4.1 to 9.6 nm. It should be noticed that, by using conventional high temperature melting technique, Liu et al. [28–30] obtained comparable average $NaYF_4$ nanocrystal radii.

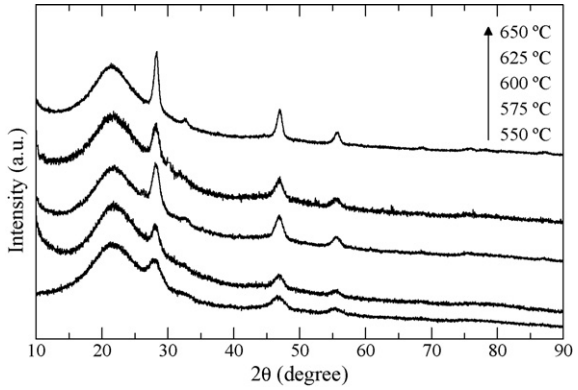

Fig. 1. XRD patterns of $95SiO_2$–$5NaYF_4$ co-doped with 0.3 Yb^{3+} and 0.1 Er^{3+} (mol%) heat-treated at indicated temperatures ranging from 550 to 650 °C.

Table 1
Calculated nanocrystals radii in $95SiO_2$–$5NaYF_4$ co-doped with 0.3 Yb^{3+} and 0.1 Er^{3+} (mol%) glass-ceramics for different temperatures of thermal treatment.

Temperature (°C)	Radii (nm)
550	4.1
575	5.6
600	6.3
625	6.7
650	9.6

3.2. Visible luminescence

In order to study luminescence properties we first present the energy level diagram of Yb^{3+} and Er^{3+} in Fig. 2. Visible emissions are indicated by down-headed arrows with corresponding wavelengths.

Excitation spectrum for the sample heat-treated at 650 °C is shown in Fig. 3a, by detecting at 540 nm assigned to the $^4S_{3/2} \rightarrow {}^4I_{15/2}$ transition of Er^{3+} ions. Corresponding emission spectrum obtained under excitation at 379 nm ($^4I_{15/2} \rightarrow {}^4G_{11/2}$ transition of Er^{3+} ions) is shown in Fig. 3b. Main green emissions can be observed in the figure at around 520–560 nm, corresponding to the $^4S_{3/2}(^2H_{11/2}) \rightarrow {}^4I_{15/2}$ Er^{3+} transitions. A weaker red emission at about 660 nm is also observed corresponding to the transition $^4F_{9/2} \rightarrow {}^4I_{15/2}$; i.e., the intensity ratio of the red to green emission bands present a value of 0.3. It can be seen that the luminescence bands show sharp structure with well-resolved Stark components, indicating that the Er^{3+} ions go into a crystalline-like environment in the ceramic sample.

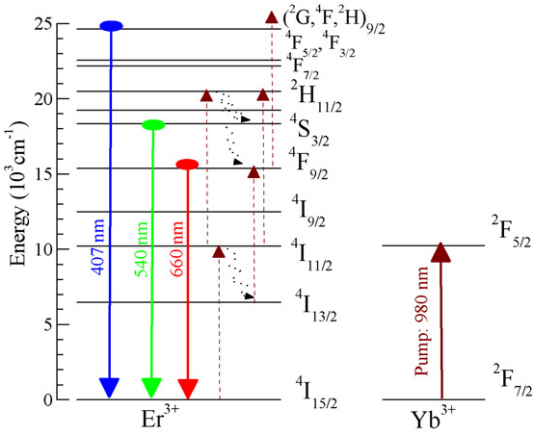

Fig. 2. Energy level diagram of Yb^{3+} and Er^{3+} ions. Up-conversion mechanisms, pumping and main emission transitions are arrowed and labelled with corresponding wavelengths.

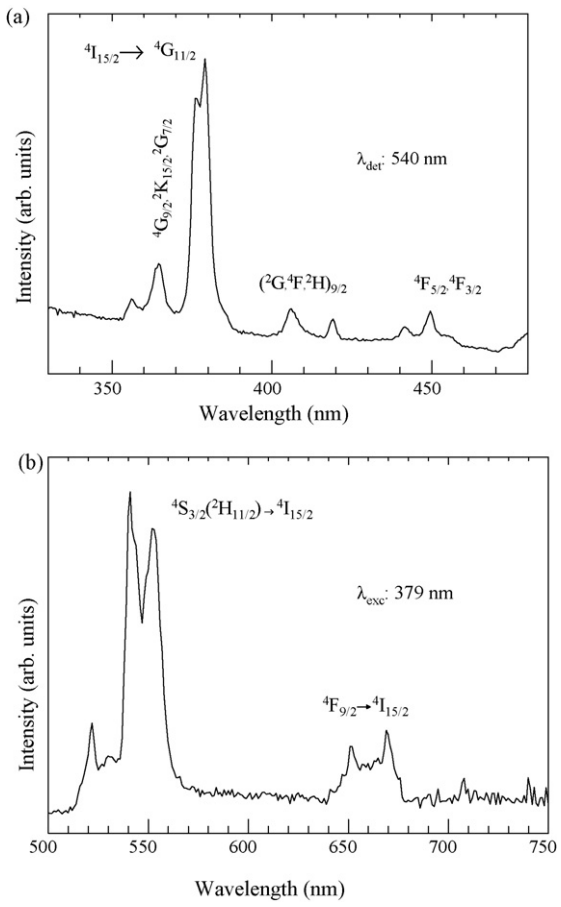

Fig. 3. Excitation (a) and emission (b) spectrum of $95SiO_2$–$5NaYF_4$ co-doped with 0.3 Yb^{3+} and 0.1 Er^{3+} (mol%) glass-ceramics heat-treated at 650 °C detecting and exciting at 540 and 379 nm, respectively. Spectra have been normalized to the maximum intensity at 379 nm (a) and 540 nm (b), respectively.

3.3. Up-conversion luminescence

Up-conversion emission spectra of the Er^{3+} ions obtained under infrared laser excitation at 980 nm with a power up to 200 mW are shown in Fig. 4a. Corresponding up-conversion mechanisms under pumping mainly the Yb^{3+} ions at 980 nm are indicated by up-headed arrows in energy level diagram, see Fig. 2. Up-conversion luminescence was perceptible by the naked eye due to its high efficiency. Up-conversion bands also show well-resolved Stark components indicating the incorporation of the RE ions into the precipitated nanocrystals. A comparison with direct excitation spectrum for the sample heat-treated at 650 °C, presented in Fig. 3b, shows an enhancement of the relative intensity of the red band due to additional population mechanism for the $^4F_{9/2}$ level in the up-conversion process. In this case the $^4F_{9/2}$ emitting level can be fed not only by the de-excitation from upper-lying levels but also by means of infrared photon absorption from intermediate up-conversion level $^4I_{13/2}$, see Fig. 2.

On the other hand, a change in the intensity ratio of the red to green up-conversion bands has been observed, from 3.21 to 0.88, with increasing of sample heat treatment temperature from 550 to 650 °C, respectively, see Fig. 4a. This change will be useful as tuneable up-conversion phosphors as will be discussed further in the next section. It can be also noticed that higher energy emissions are enhanced with increasing heat treatment temperature, like the blue emission located around 410 nm. This increase with the temperature of the heat treatment is indicative of a higher degree of crystallinity and the incorporation of larger amount of RE ions into the corresponding precipitated nanocrystals, in agreement with the behaviour observed from XRD patterns presented in Fig. 1. Thus, for the samples heat-treated at higher temperatures, i.e., 650 °C, the environment for the rare-earth ions are more crystalline-like and nonradiative relaxation rates of upper-lying levels are lower, so higher energy emissions, like the green one at around 550 nm, are favoured.

This tuneability was also observed in the 650 °C heat-treated sample for increasing pump power in the range from 10 to 200 mW, see Fig. 4b. The green to red ratio varies with excitation pump power due to the difference in up-conversion mechanisms routes. As it was above discussed, and by comparison with direct excitation spectrum, the $^4F_{9/2}$ red emitting level is fed by the de-excitation from upper-lying levels and also infrared photon absorption from intermediate up-conversion level $^4I_{13/2}$, see up-conversion mechanisms depicted in Fig. 2. Thus, different pump power dependences for population of $^4S_{3/2}(^2H_{11/2})$ and $^4F_{9/2}$ levels are expected and variation of the red to green ratio is observed in Fig. 4b.

3.4. Colour tuneability and CIE coordinates

In order to quantify the tuneability of the colour emitted by the sample, the change of the relative intensity of the up-conversion emissions has been analyzed in the framework of the CIE (Comission Internationale d'Eclairage) standard chromaticity diagram formalism [35]. This diagram represents all chromaticity visible to the human eye after a correction to sensitivity of blue, green and

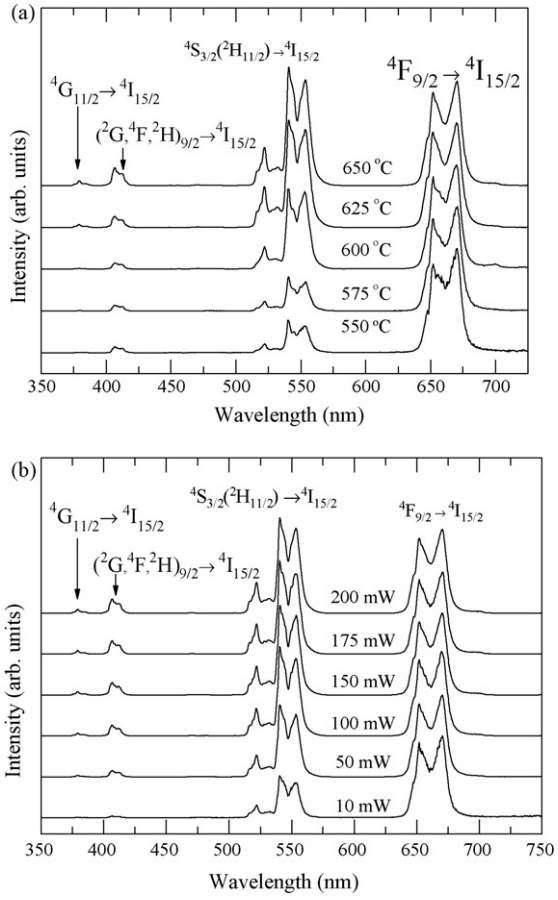

Fig. 4. Up-conversion emission spectra of $95SiO_2$–$5NaYF_4$ co-doped with 0.3 Yb^{3+} and 0.1 Er^{3+} (mol%) glass-ceramics under 980 nm excitation at 200 mW as a function of heat treatment temperature from 550 to 650 °C (a); and at 650 °C heat treatment temperature as a function of pump power from 10 to 200 mW (b). Spectra have been normalized to the maximum of the 660 nm emission band.

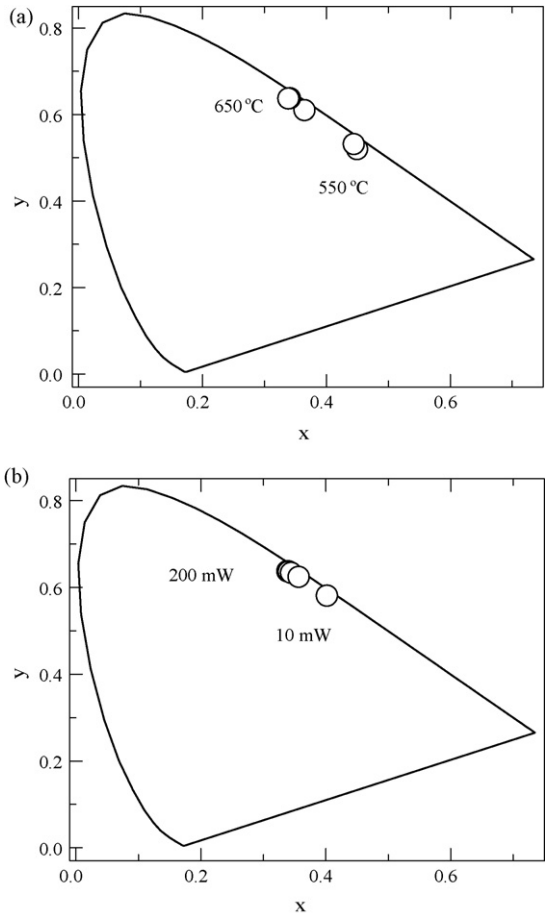

Fig. 5. CIE standard chromaticity diagram with corresponding colour coordinates of total visible up-conversion emission of the $95SiO_2$–$5NaYF_4$ co-doped with 0.3 Yb^{3+} and 0.1 Er^{3+} (mol%) glass-ceramics under 980 nm excitation (a) at 200 mW for different heat treatment temperatures ranging from 550 to 650 °C and (b) at 650 °C thermal treatment for increasing pump power ranging from 10 to 200 mW.

red receptors of the eye. The *x* and *y* axis of CIE diagram are the respective projective coordinates of the total visible luminescence. In particular, the edge of the diagram corresponds to monochromatic light whereas white light appear in the centre.

Thus, Fig. 5a presents corresponding colour coordinates obtained from up-conversion emission spectra under 980 nm infrared excitation at maximum pump power of 200 mW for different heat treatment temperatures of the sample. It can be seen how the colour gradually changes with increasing heat treatment temperature showing up the tuneability of emission colour from reddish to greenish part of the diagram. In that respect, *x* and *y* values for each sample are summarized in Table 2a, varying from (0.45, 0.52) to (0.34, 0.64) for heat treatments of 550 and 650 °C, respectively. Therefore, observed changes in the up-conversion luminescence provide a way for tuning the colour by changing heat treatment temperature of the glass-ceramic sample. Moreover, colour coordinates obtained from up-conversion emission spectra of the 650 °C heat-treated sample as function of pump power, ranging from 10 to 200 mW, shows similar values, see Table 2b, to those obtained at maximum pump power and increasing heat treatment temperature from 550 to 650 °C, see Fig. 5b.

Table 2a
CIE standard chromaticity colour coordinates, *x* and *y*, corresponding to the total visible up-conversion emission under 980 nm excitation at 200 mW of the $95SiO_2$–$5NaYF_4$ co-doped with 0.3 Yb^{3+} and 0.1 Er^{3+} (mol%) glass-ceramics for different temperatures of thermal treatment.

Temperature (°C)	*x*	*y*
550	0.45	0.52
575	0.44	0.53
600	0.36	0.61
625	0.34	0.64
650	0.34	0.64

Table 2b
CIE standard chromaticity colour coordinates, *x* and *y*, corresponding to the total visible up-conversion emission under 980 nm excitation at 650 °C heat treatment temperature of the $95SiO_2$–$5NaYF_4$ co-doped with 0.3 Yb^{3+} and 0.1 Er^{3+} (mol%) glass-ceramics for different pump powers.

Pump power (mW)	*x*	*y*
200	0.34	0.64
175	0.34	0.64
150	0.34	0.64
100	0.34	0.63
50	0.36	0.62
10	0.40	0.58

4. Conclusions

We have successfully developed nano-glass-ceramics containing Yb^{3+}–Er^{3+} co-doped $NaYF_4$ nanocrystals by thermal treatment of precursor bulk glasses obtained by the sol–gel technique, for the first time to the best of our knowledge. Precipitation of $NaYF_4$ nanocrystals has been observed by XRD patterns and the incorporation of the RE ions has been confirmed by luminescence measurements. It has been found that the intensity ratio between up-conversion emission peaks varies widely with heat treatment temperature and pump power, providing large colour tuneability. This behaviour has been explained taking into account the involved up-conversion mechanisms. This colour tuneability, which has been analyzed in terms of CIE standard chromaticity diagram formalism, opens the way for infrared tuneable up-conversion phosphors as a tool for three-dimensional optical recording and applications in photonic integrated devices.

Acknowledgments

The authors would like to thank Gobierno Autónomo de Canarias (PI042005/039), Consejería de Industria, Comercio y Nuevas Tecnologías (IDT-TF-07/077) and Ministerio de Ciencia y Tecnología of Spain Government (FIS 2006-02980) for financial support.

References

[1] Y.H. Wang, J. Ohwaki, Appl. Phys. Lett. 63 (1993) 3268.
[2] V.K. Tikhomirov, J. Koch, D. Wandt, B.N. Chichkov, Phys. Stat. Sol. (a) 202 (2005) R73.
[3] V.K. Tikhomirov, D. Furniss, I.M. Reaney, M. Beggiora, M. Ferrari, M. Montagna, R. Rolli, Appl. Phys. Lett. 81 (2002) 1937.
[4] P.A. Tick, N.F. Borreli, L.K. Cornelius, M.A. Newhouse, J. Appl. Phys. 78 (1995) 6367.
[5] J. Méndez-Ramos, V. Lavín, I.R. Martín, U.R. Rodríguez-Mendoza, V.D. Rodríguez, A.D. Lozano-Gorrín, P. Núnez, J. Appl. Phys. 94 (2003) 2295.
[6] W. Luo, Y. Wang, Y. Cheng, F. Bao, L. Zhou, Mater. Sci. Eng. B-Solid 127 (2006) 218.
[7] V.D. Rodríguez, V.K. Tikhomirov, J. Méndez-Ramos, A.B. Seddon, Europhys. Lett. 69 (2005) 128.
[8] J. Méndez-Ramos, V.K. Tikhomirov, V.D. Rodríguez, D. Furniss, J. Alloy Compd. 440 (2007) 328.
[9] H. Scheife, G. Huber, E. Heumann, S. Bär, E. Osiak, Opt. Mater. 26 (2004) 365.
[10] J.F. Suyver, J. Grimm, M.K. Van Veen, D. Biner, K.W. Krämer, H.U. Güdel, J. Lumin. 117 (2006) 1.
[11] J.F. Suyver, J. Grimm, K.W. Krämer, H.U. Güdel, J. Lumin. 114 (2005) 53.
[12] T. Trupke, A. Shalav, B.S. Richards, P. Würfel, M.A. Green, Sol. Energy Mater. Sol. C 90 (2006) 3327.
[13] A. Shalav, B.S. Richards, T. Trupke, K.W. Krämer, H.U. Güdel, Appl. Phys. Lett. 86 (2005) 013505.
[14] S.F. Lim, R. Riehn, W.S. Ryu, N. Khanarian, C.K. Tung, D. Tank, R.H. Austin, Nano Lett. 6 (2) (2006) 169.

[15] L. Wang, Y. Li, Chem. Commun. (2006) 2557.
[16] D.Y. Kong, Z.L. Wang, C.K. Lin, Z.W. Quan, Y.Y. Li, C.X. Li, Nanotechnology 18 (2007) 075601.
[17] C.J. Sun, Z. Xu, B. Hu, G.S. Yi, G.M. Chow, J. Shen, Appl. Phys. Lett. 91 (2007) 191113.
[18] X. Zhou, S. Li, X. Chen, Q. Zhu, Z. Wang, J. Zhang, J. Nanosci. Nanotechnol. 8 (2008) 1392.
[19] D.K. Chatteriee, A.J. Rufalhah, Y. Zhang, Biomaterials 29 (2008) 937.
[20] N. Menyuk, K. Dwight, J.W. Pierce, Appl. Phys. Lett. 21 (1972) 159.
[21] T. Kano, H. Yamamoto, Y. Otomo, J. Electrochem. Soc. 119 (1972) 1561.
[22] A. Bril, J.L. Sommerdijk, A.W. de Jager, J. Electrochem. Soc. 122 (1975) 660.
[23] J.L. Sommerdijk, J. Lumin. 6 (1973) 61.
[24] R.H. Page, K.I. Schaffers, P.A. Waide, J.B. Tassano, S.A. Payne, W.F. Krupke, W.K. Bischel, J. Opt. Soc. Am. B 15 (1998) 996.
[25] J.F. Suyver, A. Aebischer, D. Biner, P. Gerner, J. Grimm, S. Heer, K. Krämer, C. Reinhard, H.U. Güdel, Opt. Mater. 27 (2005) 1111.
[26] H. Naruke, T. Yamase, J. Alloy Compd. 391 (2005) 302.
[27] D. Matsuura, Appl. Phys. Lett. 81 (2002) 4526.
[28] F. Liu, E. Ma, D. Chen, Y. Yu, Y. Wang, J. Phys. Chem. B 110 (2006) 20843.
[29] F. Liu, Y. Wang, D. Chen, Y. Yu, Mater. Sci. Eng. B-Solid 136 (2007) 106.
[30] F. Liu, D. Chen, Y. Wang, E. Ma, Y. Yu, J. Alloy Compd. 443 (2007) 143.
[31] A.C. Yanes, J. Del Castillo, M. Torres, J. Peraza, V.D. Rodríguez, J. Méndez-Ramos, Appl. Phys. Lett. 85 (2004) 2343.
[32] J. Del Castillo, V.D. Rodríguez, A.C. Yanes, J. Méndez-Ramos, M.E. Torres, Nanotechnology 16 (2005) S300.
[33] V.D. Rodríguez, J. del Castillo, A.C. Yanes, J. Méndez-Ramos, M. Torres, J. Peraza, Opt. Mater. 29 (2007) 1557.
[34] S. Fujihara, C. Mochizuki, T. Kimura, J. Non-Cryst. Solids 244 (1999) 267.
[35] CIE, International Commission on Illumination, Colorimetry: Official Recommendations of the International Commission on Illumination, Publication CIE No. 15 (E-1.3.1), Bureau Central de la CIE, Paris, 1971.